Condensed Matter Physics 2008, Vol. 11, No 4(56), pp. 627–639

CONDENSED MATTER PHYSICS

Electronic structure and x-ray magnetic circular dichroism in the Heusler alloy Co_2FeSi

V.N.Antonov[1], D.A.Kukusta[1], A.P.Shpak[1], A.N.Yaresko[2]

[1] Institute for Metal Physics of the National Academy of Sciences of Ukraine, 36 Vernadsky Str., 03142 Kiev
[2] Max-Planck-Institut für Festkörperforschung, Heisenbergstrasse 1, D–70569 Stuttgart, Germany

Received December 11, 2007, in final form June 18, 2008

The electronic structure and x-ray magnetic circular dichroism (XMCD) spectra of the Heusler alloy Co_2FeSi were investigated theoretically from first principles, using the fully relativistic Dirac linear MT-orbital (LMTO) band structure method. Densities of valence states, orbital and spin magnetic moments as well as polarization of the electronic states at the Fermi level are analyzed and discussed. The origin of the XMCD spectra in the Co_2FeSi compound is examined. The calculated results are compared with available experimental data.

Key words: *strongly correlated systems, electronic structure, x-ray magnetic circular dichroism*

PACS: *71.28.+d, 71.25.Pi, 75.30.Mb*

1. Introduction

Electronic devices exploiting the spin of an electron have attracted great scientific interest [1]. Their basic element is a ferromagnetic electrode providing a spin-polarized electric current. In this context, the most interesting materials are the ones having a complete spin-polarization at the Fermi level. The rapid development of magneto-electronics intensified the interest to such materials. The application of the spin degree of freedom to conventional electronic devices has got several advantages such as non-volatility, an increased data processing speed, a decreased electric power consumption and increased integration densities [1,2]. The current advances in new materials are promising for engineering new spintronic devices in the near future [2].

A metal for spin-up and a semiconductor for spin-down electrons is called half-metallic ferromagnet (HMF) [3], and Heusler compounds have been considered potential candidates to show this property. de Groot *et al.* first predicted half-metallic ferromagnetism for the Heusler-like compound NiMnSb [3]. The full Heusler alloys are defined as well-ordered ternary intermetallic compounds, at the stoichiometric composition X_2YZ, which have the cubic $L2_1$ structure. These compounds involve two different transition metal atoms X, and Y, and a third element Z which is a non-magnetic metal or nonmetallic element. Currently the Heusler alloys are at the focus of a large scientific interest due to their potential for applications in magnetic field sensors and spintronic devices [1]. Numerous theoretical and experimental studies of Heusler alloys have been carried out, and it has been shown that composition and heat treatment are important parameters determining their magnetic properties.

In this paper we investigate the Heusler alloy Co_2FeSi. This compound is one of the most promising candidates for spintronic applications. Recently, Balke *et al.* [4] have conclusively showed that Co_2FeSi crystallizes in the ordered $L2_1$ structure. Balke *et al.* [5] revealed that Co_2FeSi undergoes the $L2_1 \leftrightarrow B2$ phase transition at the temperature ≈ 1031 K. Wurmehl *et al.* [6] have found that $L2_1$-ordered Co_2FeSi is the Heusler compound as well as the half-metallic ferromagnet with the highest Curie temperature (1100 ± 20 K) in the classes of Heusler compounds and half-metallic ferromagnets. The measured magnetic moment in saturation was found to be 5.97 ± 0.05 μ_B at 5 K which corresponds to 1.49 μ_B per atom. An extrapolation to 0 K gives an integer magnetic moment of $6\,\mu_B$ per unit cell within the experimental uncertainty, as expected for a half-metallic ferromagnet. Mössbauer spectroscopy was performed at magnetostructural investigations, the observed pattern of the spectrum being typical of a magnetically ordered system. Moreover, XMCD spectra taken at the $L_{2,3}$ absorption edges of Fe and Co at photoabsorption were used in order to investigate the site specific magnetic properties. Schneider *et al.* [7] have grown thin films of Co_2FeSi and provided their full experimental characterization including the measurements of the x-ray absorption spectra (XAS) as well as the XMCD spectra. They estimated the element-specific spin and orbital magnetic moments using sum rules. Furthermore, investigations of integral macroscopic magnetic transport properties, such as the magnetization, resistivity, magnetoresistance, and spin polarization of Co_2FeSi films were carried out. The authors found out that the saturation magnetization of the films does not depend on the substrate chosen and exhibits a $T^{3/2}$ behavior over the 0–300 K interval. It can be extrapolated to 5.0 μ_B/f.u. at 0 K. This value is much smaller than the value of saturation magnetization observed on the bulk sample [6]. That might be caused by an incomplete atomic order in thin films with respect to the $L2_1$ structure. Schneider *et al.* [7] also estimated the surface spin polarization using the spin-resolved photoemission spectroscopy. They found quite small spin polarization at E_F in Co_2FeSi thin films (≈6%). This value is drastically reduced with respect to the expected 100% in case of half-metallic behavior as predicted in [6]. It has been shown that the observed reduction of spin polarization at E_F is not confined to the outermost surface layer and originates from disorder effects which introduce minority states at E_F. Resistivity measured over all 0–300 K temperature interval revealed metallic behavior of Co_2FeSi thin films. Anisotropic magnetoresistance effect with respect to the current direction was also observed which implies a significant contribution of spin-flip scattering process to the magnetoresistance. X-ray magnetic circular dichroism photoemission electron microscopy has been used for a direct observation of the domain structure of single- and polycrystalline samples of Co_2FeSi in [8]. Spin polarized photoemission from a single domain of single crystal shows a spin polarization of 16% at the Fermi energy and up to 35% in the *d*-bands, at room temperature.

Despite a failure to reach 100% polarization at the Fermi level and relatively small saturation magnetization, thin films of Co_2FeSi have been successfully used for fabrication of magnetic tunnel junctions [9]. The tunnel magneto-resistance (TMR) ratios of 60% at low temperature and 41% at room temperature suggest that an improvement in the materials is still necessary for a successful use in the devices [8].

Theoretically, the electronic structure and other properties of Co_2FeSi were studied in [5,6,10, 11]. Self-consistent band-structure calculations were carried out by Kandpal *et al.* using the full-potential linear augmented-plane-wave (FLAPW) method [10]. The main focus in [10] was made on the magnetic moment and on its very strong discrepancy while comparing the experimental and the calculated values for Co_2FeSi. Wurmehl *et al.* [6] systematically investigate the effect of different approximations to the exchange-correlation potential as well as of different band structure methods on the magnetic moments in Co_2FeSi. They used LMTO method, the FLAPW method and the Korringa-Kohn-Rostocker (KKR) method. The latter method was allowed to calculate the band structure in the muffin-tin (MT) and the atomic sphere (ASA) approximations. Moreover, it provides the coherent potential approximation (CPA) to be used for disordered systems. The calculations were carried out with the most common parameterizations of the exchange-correlation functional as given by Moruzzi, Janak, and Williams [12], von Barth and Hedin [13], Vosco, Wilk, and Nussair [14], and Engel and Vosko [15]. The generalized gradient approximation (GGA) was used in the form given by Perdew *et al.* [16,17]. The calculated total magnetic moments range from $4.9\,\mu_B$ to $5.7\,\mu_B$ in the LSDA approximation. Thus, they are throughout too low compared to the experiment. Therefore, the LSDA band structure calculations are not sufficient to reproduce half-metalicity in Co_2FeSi. However, the LSDA+U scheme satisfactorily reproduces the experimental observations. Values of U_{eff} from 2.5 eV to 5.0 eV for Co and 2.4 eV to 4.8 eV for Fe result in a magnetic moment of 6 μ_B and a gap in the minority states. Finally, it was shown for Co_2FeSi that correlation could also contribute to the destruction of the half-metallic behavior if the correlation becomes as strong as 5 eV. The substitutional series of the quaternary Heusler compound $Co_2Mn_{1-x}Fe_xSi$ (x=0, 0.5, 1) was synthesized and investigated both experimentally and theoretically by Balke *et al.* [5]. The structural and magnetic properties of the $Co_2Mn_{1-x}Fe_xSi$ Heusler alloys were investigated by means of x-ray diffraction, high- and low-temperature magnetometry, Mössbauer spectroscopy, and differential scanning calorimetry. The electronic structure was explored by means of high energy photoemission spectroscopy at about 8 keV photon energy. To calculate the electronic and magnetic structures they used the FLAPW method. All the compounds under consideration were found to be half-metallic in the LDA+U approach. Sargolzaei *et al.* [18] have carried out density functional calculations of Co_2YZ (Y = Mn,Fe; Z = Al, Si,Ga,Ge) using the relativistic version of the full-potential local-orbital (FPLO) minimum-basis band-structure method and the Perdew-Wang parameterization of the exchange-correlation potential in the LSDA approach. The authors optimized the equilibrium lattice parameters using LSDA total-energy calculations. The calculated lattice constants a turned out to be 2–3% smaller than the experimental values. It was found that Co_2FeSi shows considerably different magnetic moments at the LSDA and experimental lattice constants. It originates from the fact that at the theoretical lattice constant, the Fermi level is situated in a steep slope at the band edge of an almost empty minority spin $3d$ band, and flat minority spin energy bands cross the Fermi level in Co_2FeSi. The latter gives rise to the mentioned steep band edge and thus to the sensitivity of the magnetic moment of Co_2FeSi with respect to the lattice spacing. It was found that spin-orbit coupling reduces the degree of spin polarization of the density of states at Fermi level by a few percent. The authors present an alternative explanation of the measured integer total moment of Co_2FeSi, contrasting the suggested correlation-induced half-metalicity. While the LDA+U approach yields a half-metallic state with an integer total moment at the experimental lattice constant, the LSDA+OP approach yields the experimental total moment at a 2.0% expanded lattice constant. The authors propose that the measured moment of Co_2FeSi need not be caused by a correlated half-metallic state. It could, e.g., arise from a small but influential disorder of the sample.

The effect of different types of disorder on properties of Co_2FeSi was investigated by Nakatani *et al.* [11]. It turned out that in Co_2FeSi E_F lies close to the upper edge of the gap, near the minimum energy of the conduction band. In such a case, the half-metalicity can be spoiled by the increase of temperature and structural disorder because some types of disorder (B2- and A2-type) form additional states in the minority gap. A perfect $L2_1$ structure assumed for all the above calculations is not present in real samples; disorders are usually expected. This important fact was considered in calculations [11]. The investigations of the disordering effects on the electronic structure of Co_2FeSi alloy have shown that moderate disordering between Fe, Co, and Si atoms forms additional electronic states near the gap edge, which immediately destroys the half-metalicity and reduces spin-polarization at E_F level. This indicates that a higher spin polarization can be achieved with a higher degree of order.

In the present study, we focus our attention on the x-ray magnetic circular dichroism in the Heusler alloy Co_2FeSi. The XMCD technique developed in recent years has evolved into a powerful magnetometry tool to separate orbital and spin contributions into the element specific magnetic moments. XMCD experiments measure the absorption of x-rays with opposite (left and right) states of circular polarization. Recently x-ray magnetic circular dichroism in the ferromagnetic Co_2FeSi alloy has been measured at the Co and Fe $L_{2,3}$ edges for the bulk [6] and thin film samples [7]. These two measurements gave almost similar results in the shape of the XAS and XMCD spectra.

This paper is organized as follows. Section 2 presents a description of the Heusler alloys Co_2FeSi crystal structure and the computational details. Section 3 is devoted to the electronic structure and XMCD spectra of the Co_2FeSi compound calculated in the fully relativistic Dirac LMTO band structure method. The calculated results are compared with the available experimental data. Finally, the results are summarized in section 4.

2. Crystal structure and computational details

The Heusler-type X_2YZ compound crystallizes in the cubic $L2_1$ structure with $Fm\overline{3}m$ space group (No. 225). It is formed by four interpenetrating fcc sublattices as shown in figure 1. The X ions occupy the $8c$ Wyckoff positions ($x = \frac{1}{4}$, $y = \frac{1}{4}$, $z = \frac{1}{4}$). The Y ions occupy the $4a$ positions (x=0, y=0, z=0), and the Z ions are placed at the $4b$ sites ($x = \frac{1}{2}$, $y = \frac{1}{2}$, $z = \frac{1}{2}$). All atoms have eight nearest neighbors at the same distance. The Y and Z atoms have eight X atoms as nearest neighbors, while for X there are four Y and four Z atoms.

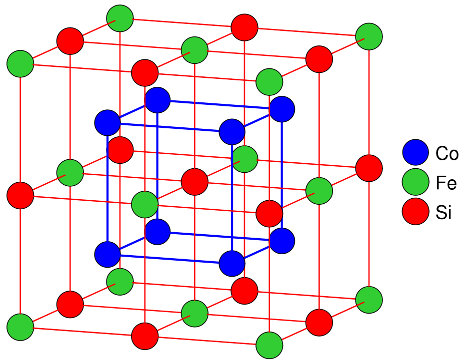

Figure 1. (Color online) Schematic representation of the $L2_1$ structure. The cubic cell contains four primitive cells.

Using straightforward symmetry considerations it can be shown that all magneto-optical phenomena (XMCD, MO Kerr and Faraday effects) are caused by the symmetry reduction, in comparison to the paramagnetic state, caused by magnetic ordering [19]. This symmetry lowering occurs only when spin-orbit (SO) coupling is included. Therefore, in order to calculate the XMCD properties one has to account for both magnetism and SO coupling at the same time.

Within the one-particle approximation, the absorption coefficient μ for incident x-rays is determined by the probability of electron transitions from an initial core state (with wave function ψ_j and energy E_j) to final unoccupied states (with wave functions $\psi_{n\mathbf{k}}$ and energies $E_{n\mathbf{k}}$) as

$$\mu_j^{\lambda}(\omega) = \sum_{n\mathbf{k}} |\langle \Psi_{n\mathbf{k}} | \mathcal{J}_\lambda | \Psi_j \rangle|^2 \delta(E_{n\mathbf{k}} - E_j - \hbar\omega)\theta(E_{n\mathbf{k}} - E_{\mathrm{F}}) \,, \tag{1}$$

where $\hbar\omega$ is the photon energy, λ is its polarization and $\mathcal{J}_\lambda = -e\boldsymbol{\alpha}\mathbf{a}_\lambda$ being the dipole electron-photon interaction operator, $\boldsymbol{\alpha}$ are Dirac matrices, $\mathbf{a}_\lambda$ is the λ polarization unit vector of the photon vector potential $[a_\pm = 1/\sqrt{2}(1, \pm i, 0), a_z = (0, 0, 1)]$. (Here $+/-$ denotes, respectively, left and right circular photon polarizations with respect to the magnetization direction in the solid).

In order to simplify the comparison of the theoretical x-ray isotropic absorption $L_{2,3}$ spectra of Co_2FeSi to the experimental ones we take into account the background intensity which affects the high energy part of the spectra and is caused by different kind of inelastic scattering of the electron promoted to the conduction band above Fermi level due to x-ray absorption (scattering on potentials of surrounding atoms, defects, phonons etc.). To calculate the background spectra we used the model proposed by Richtmyer *et al.* [20]. The absorption coefficient for the background intensity is

$$\mu(\omega) = \frac{C\Gamma_{\mathrm{c}}}{2\pi} \int_{E_{cf_0}}^{\infty} \frac{\mathrm{d}E_{\mathrm{cf}}}{(\Gamma_{\mathrm{c}}/2)^2 + (\hbar\omega - E_{\mathrm{cf}})^2} \,, \tag{2}$$

where $E_{\mathrm{cf}} = E_{\mathrm{c}} - E_{\mathrm{f}}$, E_{c}, and Γ_{c} are the energy and the lifetimes broadening of the core hole, E_{f} is the energy of empty continuum level, E_{f_0} is the energy of the lowest unoccupied continuum level, and C is a normalization constant which in this paper has been used as an adjustable parameter.

We have adopted the LSDA+U method [21] as a different level of approximation to treat the electron-electron correlations. We used the rotationally invariant LSDA+U method. This method is described in detail in previous paper [22]. The effective on-site Coulomb repulsion U was considered as an adjustable parameter. We used $U = 4.0$ eV. For this value, we found good agreement between the calculated and the extrapolated value of total spin magnetic moment of Co_2FeSi [6]. For the exchange integral J, the value of 0.89 eV estimated from constrained LSDA calculations was used.

Concurrent with the development of the x-ray magnetic circular dichroism experiment, some important magneto-optical sum rules have been derived [23–26].

For the $L_{2,3}$ edges the l_z sum rule can be written as [27]

$$\langle l_z \rangle = n_h \, \frac{4}{3} \, \frac{\int_{L_3+L_2} \mathrm{d}\omega(\mu_+ - \mu_-)}{\int_{L_3+L_2} \mathrm{d}\omega(\mu_+ + \mu_-)} \,, \tag{3}$$

where n_h is the number of holes in the d band $n_h = 10 - n_d$, $\langle l_z \rangle$ is the average of the magnetic quantum number of the orbital angular momentum. The integration is taken over the whole $2p$ absorption region. The s_z sum rule can be written as

$$\langle s_z \rangle + \frac{7}{2}\langle t_z \rangle = n_h \, \frac{\int_{L_3} \mathrm{d}\omega(\mu_+ - \mu_-) - 2\int_{L_2} \mathrm{d}\omega(\mu_+ - \mu_-)}{\int_{L_3+L_2} \mathrm{d}\omega(\mu_+ + \mu_-)} \,, \tag{4}$$

where t_z is the z component of the magnetic dipole operator $\mathbf{t} = \mathbf{s} - 3\,\mathbf{r}\,(\mathbf{r}\cdot\mathbf{s})/|\mathbf{r}|^2$ which accounts for the asphericity of the spin moment. The integration $\int_{L_3} \left(\int_{L_2}\right)$ is taken only over the $2p_{3/2}$ $\left(2p_{1/2}\right)$ absorption region.

The details of the computational method are described in the previous papers [28–31], and here we only mention some aspects specific to the present calculations. The calculations were performed for the experimentally observed lattice constant $a = 5.658$ Å[32] as well as for the one theoretically calculated in total energy optimization using the spin-polarized fully relativistic linear-muffin-tin-orbital (SPR LMTO) method [33,34] with the combined correction term taken into account. The LSDA part of the calculations was based on the spin-density functional with the Perdew-Wang [35] of the exchange-correlation potential. Brillouin zone (BZ) integrations were performed using the improved tetrahedron method [36] and charge self-consistency was obtained on a grid of 349 $\mathbf{k}$ points in the irreducible part of the BZ. The basis consisted of transition metal s, p, d and Si s, p and d LMTO's.

The intrinsic broadening mechanisms have been accounted for by folding the XMCD spectra with a Lorentzian. For the finite lifetime of the core hole, a constant width Γ_c, in general from [37], has been used. The finite apparative resolution of the spectrometer has been accounted for by a Gaussian of 1.0 eV.

3. Results and discussion

3.1. Energy band structure

The total and partial DOS's of Co_2FeSi calculated in the LSDA approximation are presented in figure 2 for the experimentally measured lattice constant. The occupied part of the valence band can be subdivided into several regions. Si $2s$ states appear between -12.0 eV and -9.0 eV. The states in the energy range from -7.0 eV to 2.0 eV are formed by Co and Fe d states and Si p states. Our calculations show that Co_2FeSi has local spin magnetic moments of $1.224\,\mu_\mathrm{B}$ on Co, $2.709\,\mu_\mathrm{B}$ on Fe and $-0.033\,\mu_\mathrm{B}$ on Si. The orbital moments are equal to $0.049\,\mu_\mathrm{B}$, $0.080\,\mu_\mathrm{B}$, and $0.002\,\mu_\mathrm{B}$ on the Co, Fe, and Si sites, respectively. The interaction between the transition metals is ferromagnetic which leads to a total calculated moment of $5.125\,\mu_\mathrm{B}$. This value is in good agreement with previous calculations [7,10] and differs from the experimental value of $6.00\pm0.05\ \mu_\mathrm{B}$ [6].

The crystal field at the Co $8c$ site (T_d point symmetry) causes the splitting of d orbitals into a doublet e ($3z^2-1$ and x^2-y^2) and a triplet t_2 (xy, yz, and xz). The crystal field at the Fe $4a$ site (O_h point symmetry) splits Fe d states into e_g ($3z^2-1$ and x^2-y^2) and t_{2g} (xy, yz, and xz) states. The hybridization between Fe and Co d states plays an important role in the formation of the band structure of Co_2FeSi. It leads to the splitting of the d states into the bonding states which are of Co and Fe d character and antibonding states with stronger contribution of Fe d states.

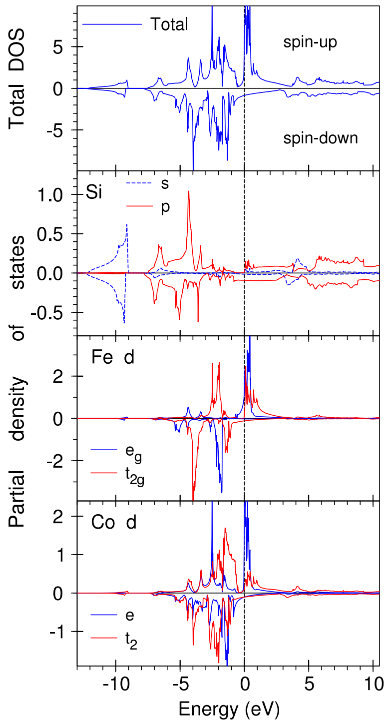

Figure 2. (Color online) The total (in states/(cell eV)) and partial (in states/(atom eV)) density of states of Co_2FeSi. The Fermi energy is at zero.

Figure 3 shows the band structure and density of states calculated using the LSDA+U method. The effective Coulomb-exchange parameters $U_{\rm eff}$ were set to 3.11 eV at the Co and Fe sites (U= 4 eV and J= 0.89 eV). The minority DOS figure 3 exhibits a clear gap around $E_{\rm F}$. Thus, according to the spin-polarized LSDA+U calculations Co_2FeSi is a half-metallic ferromagnet if the spin-orbit coupling is neglected. The high density below $E_{\rm F}$ is dominated by d states being located at Co and Fe sites. Inspecting the majority DOS, one finds a small density of states near $E_{\rm F}$. This density is mainly derived from the states located at Co and Si sites. Although spin-orbit splitting of the d energy bands for both the Co and Fe atoms is much smaller than their spin and crystal-field splittings, this interaction destroys the energy gap for the minority spin states. The Fermi level falls within a region of very small but finite minority-spin DOS. In this case the spin polarization of electron states at the Fermi energy is equal to 94.5%. Similar results were obtained in [38,39] for some other Heusler alloys. The authors show that the spin-orbit interaction can cause a nonvanishing density of states within the minority-spin band gap of half-metals around the Fermi level and reduce the spin polarization at the $E_{\rm F}$. Due to closing, the gap total spin magnetic moment became equal to 5.99 $\mu_{\rm B}$, slightly less than integer value predicted in [6].

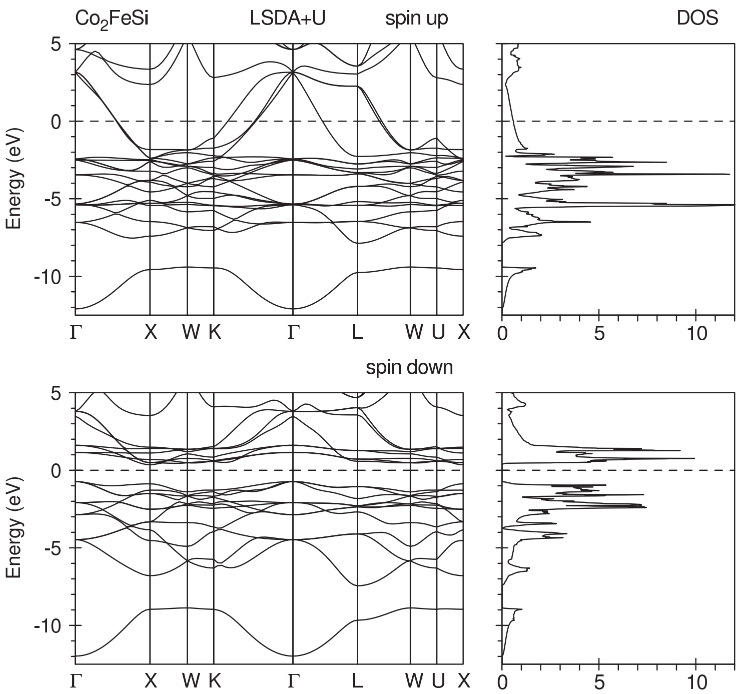

Figure 3. Band structure of Co_2FeSi calculated in LSDA+U approximation. The Fermi energy is at zero.

3.2. XMCD spectra

At the core level edge XMCD is not only element-specific but also orbital specific. For $3d$ transition metals, the electronic states can be probed by the K, $L_{2,3}$ and $M_{2,3}$ x-ray absorption and emission spectra. Recently x-ray magnetic circular dichroism in the ferromagnetic Co_2FeSi alloy has been measured at the Co and Fe $L_{2,3}$ edges [7]. The experimentally measured dichroic lines have different signs at the L_3 and L_2 edges of Co and Fe [7].

In order to compare relative amplitudes of the L_3 and L_2 XMCD spectra we first normalize the corresponding x-ray absorption spectra for the right polarized x-rays μ^- to the experimental ones taking into account the background scattering intensity as described in section 2. Figure 4 shows the XAS and XMCD spectra at the $L_{2,3}$ edges of Co calculated in the LSDA+U approach together with the experimental data [7]. The corresponding spectra for Fe are presented in figure 5. The contribution from the background scattering is shown by dotted line in the upper panel in figures 4 and 5.

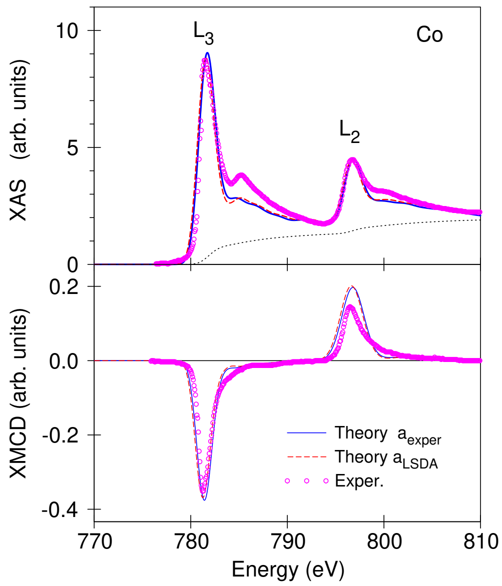

Figure 4. (Color online) Upper panel: calculated in LSDA+U approximation for the experimental a_{expr} (blue full line) and theoretical a_{theory} (red dashed lines) values of lattice parameter, as well as experimental (circles) x-ray absorption spectra for the right polarized x-rays μ^- of Co_2FeSi at the Co $L_{2,3}$ edges. Experimental spectra [7] were measured by means of total photoelectron yield with external magnetic field (1.6 T). Dotted line shows the theoretically calculated background spectra. Low panel: theoretically calculated for the experimental a_{expr} (blue thin full line) and theoretical a_{theory} (red dashed lines) values of lattice parameter and experimental [7] (circles) XMCD spectra of Co_2FeSi at the Co $L_{2,3}$ edges.

Due to the dipole selection rules, apart from the $4s_{1/2}$ states (which have a small contribution to the XAS due to relatively small $2p \to 4s$ matrix elements) only $3d_{3/2}$ states occur as final states for L_2 XAS for unpolarized radiation, whereas for the L_3 XAS, the $3d_{5/2}$ states also contribute [27]. Although the $2p_{3/2} \to 3d_{3/2}$ radial matrix elements are only slightly smaller than for the $2p_{3/2} \to 3d_{5/2}$ transitions, the angular matrix elements strongly suppress the $2p_{3/2} \to 3d_{3/2}$ contribution [27]. Therefore, neglecting the energy dependence of the radial matrix elements, the L_2 and the L_3 spectrum can be viewed as a direct mapping of the DOS curve for $3d_{3/2}$ and $3d_{5/2}$ character, respectively.

The experimental Co XAS has a pronounced shoulder at the L_3 peak at around 785 eV shifted by about 3 eV with respect to the maximum to higher photon energy. This structure is less pronounced at the L_2 edge. This result can be ascribed to the lifetime broadening effect because

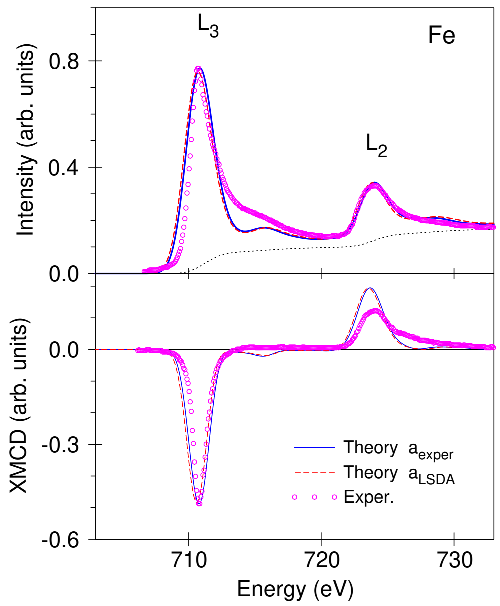

Figure 5. (Color online) Upper panel: calculated in LSDA+U approximation for experimental $a_{\rm expr}$ (blue full line) and theoretical $a_{\rm theory}$ values of lattice parameter (red dashed line), as well as experimental (circles) x-ray absorption spectra for the right polarized x-rays μ^- of Co_2FeSi at the Fe $L_{2,3}$ edges. Experimental spectra [7] were measured by means of total photoelectron yield with external magnetic field (1.6 T). Dotted line shows the theoretically calculated background spectra. Low panel: theoretically calculated for experimental $a_{\rm expr}$ (blue full line) and theoretical $a_{\rm theory}$ values of lattice parameter (red dashed line) and experimental [7] (circles) XMCD spectra of Co_2FeSi at the Fe $L_{2,3}$ edges.

the lifetime of the $2p_{1/2}$ core hole is shorter than the $2p_{3/2}$ core hole due to the L_2L_3V Coster-Kronig decay. This feature is partly due to the interband transitions from $2p$ core level to Co $3d$ empty states at around 4 eV above the Fermi level. Actually, as can be seen in figure 6, Co d partial DOS's have two pronounced peaks at 4 eV and approximately 6 eV above the Fermi level. Both the features are reflected in the theoretically calculated XAS at the Co L_3 edge around 785 and 789 eV, respectively (figure 4), although the second peak is less pronounced in the experimental spectrum.

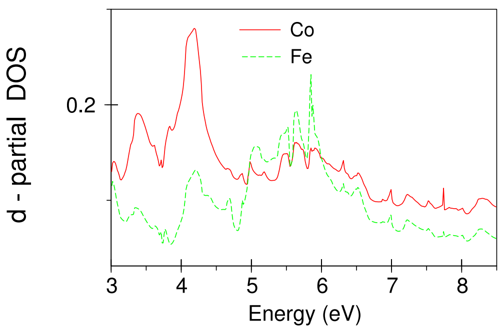

Figure 6. (Color online) The Co and Fe d-partial density of unoccupied states (in states/(atom eV)) of Co_2FeSi. Energies are relative to the Fermi energy.

Figure 5 presents the calculated XAS as well as XMCD spectra of the Co_2FeSi compound at the Fe $L_{2,3}$ edges compared with the experimental data [7]. The peak in the empty Fe d partial

DOS at 5.8 eV above the Fermi level is less intensive in comparison with the corresponding peak in the Co d partial DOS (see figure 6). Therefore, the theoretically calculated XAS has only one pronounced feature at the high energy part of the XAS at 717 eV (figure 5).

It may be seen in the upper part of figure 4 that the experimentally measured Co L_3 XAS has some additional intensity around 785 eV which is not completely reproduced by the theoretical calculations. A similar situation also appears in the Fe L_3 XAS (figure 5) where the theoretical one-particle calculations do not reproduce all the intensity at around 717 eV. This might indicate that additional satellite structures may appear due to many-body effects at the high energy tails of both the Co and Fe $L_{2,3}$ XAS's. This issue needs additional theoretical investigation using an appropriate many-body treatment.

The XMCD spectra at the $L_{2,3}$ edges are mostly determined by the strength of the SO coupling of the initial $2p$ core states and spin-polarization of the final empty $3d_{3/2}$ and $3d_{5/2}$ states while the exchange splitting of the $2p$ core states as well as the SO coupling of the $3d$ valence states are of minor importance for the XMCD at the $L_{2,3}$ edge of $3d$ transition metals [27]. The calculated Co and Fe $L_{2,3}$ XMCD spectra are in good agreement with the experiment [7], although the calculated magnetic dichroism is somewhat too high at the L_2 edge. One of the reasons for this discrepancy might be the core-hole effect. When the $2p$ core electron is photo-excited to the unoccupied d states, the distribution of the charge changes to account for the created hole. This effect is not taken into account in the method we used for the electronic structure calculations, and it is likely to lead to the observed discrepancy [40].

To investigate the effect of lattice constant on the magnetic moments and XMCD spectra we optimized the equilibrium lattice parameter a using LSDA total-energy calculations. The calculated lattice constant a=5.545 Å is 2% smaller than the experimental value a=5.658 Å. Similar results were obtained by Sargolzaei *et al.* [18]. For the theoretically calculated LSDA lattice constant, spin magnetic moments are reduced by approximately 7% and 4% for Co and Fe, respectively. However, LSDA+U approach still produces a half-metallic solution for the theoretically calculated lattice constant. We found that the XMCD spectra are almost identical for the LSDA and experimentally measured lattice constants (figures 4 and 5).

3.3. Magnetic moments

In magnets, the atomic spin M_s and orbital M_l magnetic moments are basic quantities. Therefore, their separate determination is important. Methods of their experimental determination include traditional gyromagnetic ratio measurements [41], magnetic form factor measurements using neutron scattering [42], and magnetic x-ray scattering [43]. In addition to these, the recently developed x-ray magnetic circular dichroism combined with several sum rules [23–26] has attracted much attention as a method of site- and symmetry-selective determination of M_s and M_l.

Due to significant implications of the sum rules, numerous experimental and theoretical studies have been reported aimed at investigating their validity for itinerant magnetic systems, but with widely different conclusions. The claimed adequacy of the sum rules varies from very good (within 5% agreement) to very poor (up to 50% discrepancy) [27]. This lack of a consensus may have several origins. For example, on the theoretical side, it has been demonstrated by circularly polarized $2p$ resonant photoemission measurements of Ni that both the band structure effects and electron-electron correlations are needed to satisfactorily account for the observed XMCD spectra [44]. However, it is extremely difficult to include both of them in a single theoretical framework. Besides, the XAS as well as XMCD spectra can be strongly affected (especially for the early transition metals) by the interaction of the excited electron with the created core hole [40,45].

On the experimental side, the indirect x-ray absorption techniques, i.e., the total electron and fluorescence yield methods, are known to suffer from saturation and self-absorption effects that are very difficult to correct for [46]. The total electron yield method can be sensitive to the varying applied magnetic field, changing the electron detecting efficiency, or, equivalently, the sample photocurrent. The fluorescence yield method is insensitive to the applied field, but the yield is intrinsically not proportional to the absorption cross section, because the radiative to non-radiative relative core-hole decay probability strongly depends on the symmetry and spin

Table 1. The experimental measured (using transmition mode (TM) and total electron yield (TEY) methods) and calculated (for the experimentally measured lattice constant) spin M_s, orbital M_l total M_s+M_l magnetic moments (in μ_B) of $\mathrm{Co_2FeSi}$ (sum rules[1] applied for the XMCD spectra calculated neglecting the energy dependence of the radial matrix elements, sum rules[2] applied for the XMCD spectra calculated neglecting the energy dependence of the radial matrix elements and neglecting $p \to s$ transitions).

method	atom	M_s	M_l	M_s+M_l
LSDA	Si	–0.033	0.002	–0.031
	Co	1.224	0.049	1.273
	Fe	2.709	0.080	2.789
LSDA+OP	Si	–0.025	0.002	–0.023
	Co	1.293	0.059	1.352
	Fe	2.717	0.123	2.840
LSDA+U	Si	–0.036	0.008	–0.028
	Co	1.622	0.111	1.733
	Fe	2.663	0.145	2.808
Sum rules	Co	1.122	0.072	1.194
	Fe	1.861	0.096	1.957
Sum rules[1]	Co	1.526	0.110	1.636
	Fe	2.363	0.141	2.504
Sum rules[2]	Co	1.554	0.112	1.666
	Fe	2.394	0.144	2.538
Expt. (TM)[6] bulk sample	Co	1.2 ± 0.1		
	Fe	2.6 ± 0.1		
Expt. (TM) [7] thin films	Co	1.25 ÷ 1.28	0.11 ÷ 0.13	1.36 ÷ 1.41
	Fe	2.43 ÷ 2.46	0.07 ÷ 0.12	2.50 ÷ 2.58
Expt. (TEY)[7] thin films	Co	1.07 ÷ 1.13	0.04 ÷ 0.14	1.11 ÷ 1.27
	Fe	2.46 ÷ 2.47	0.05 ÷ 0.10	2.51 ÷ 2.57

polarization of the XAS final states [47].

The Fe L_3 and L_2 spectra in $\mathrm{Co_2FeSi}$ are strongly overlapped. Therefore, the decomposition of a corresponding experimental $L_{2,3}$ spectrum into its L_3 and L_2 parts is quite difficult and can lead to a significant error in the estimation of the magnetic moments using the sum rules (the integration $\int_{L_3}$ and $\int_{L_2}$ in equation (4) should be taken over the $2p_{3/2}$ and $2p_{1/2}$ absorption regions separately). Besides, the experimentally measured Co and Fe $L_{2,3}$ x-ray absorption spectra have background scattering intensity and the integration of the corresponding XASs may lead to an additional error in the estimation of the magnetic moments using the sum rules.

The value of the orbital magnetic moments derived from the experimental XMCD spectra is considerably higher in comparison with our LSDA band structure calculations (Table 1). It is a well-known fact, however, that LSDA calculations are inaccurate in describing orbital magnetism [48,27]. In the LSDA, the Kohn-Sham equation is described by a local potential which depends on the electron spin density. The orbital current, which is responsible for M_l, is, however, not included in the equations. This means that although M_s is self-consistently determined in the LSDA, there is no framework to determine simultaneously M_l self-consistently. Numerous attempts have been made to better estimate $\mathrm{M_l}$ in solids. They can be roughly classified into two categories. One is based on the so-called current density functional theory [49–51] which is intended to extend density functional theory to include the orbital current as an extra degree of freedom, which describes M_l. Unfortunately an explicit form of the current density functional is at present unknown. The other category includes orbital polarization [52–55], self-interaction correction [56], and LSDA+U [57,22] approaches.

To calculate M_l beyond the LSDA scheme we used the rotationally invariant LSDA+U method

[22] using a double-counting correction term in the fully-localized limit approximation [58,59]. We used $U = J = -0.89$ eV for the transition metal sites. In this case $U_{\rm eff} = U - J = 0$ and the effect of the LSDA+U comes from non-spherical terms which are determined by F^2 and F^4 Slater integrals. This approach is similar to the orbital polarization (OP) correction [27]. The LSDA+OP calculations (LSDA+U with $U_{\rm eff} = 0$) produce orbital magnetic moments equal to 0.059 μ_B and 0.123 μ_B for Co and Fe sites, respectively. The Co LSDA+OP orbital moment is somewhat smaller than the experimental estimates. However, the value for Fe is in good agreement with the experimental data. A full LSDA+U method produces larger orbital magnetic moments (0.111 μ_B and 0.145 μ_B for Co and Fe sites, respectively). We should mention that the shape of the XMCD spectra in Co_2FeSi is less sensitive to the orbital polarization correction in comparison with the evaluated orbital magnetic moments. The XAS and XMCD spectra calculated in the LSDA, LSDA+OP and LSDA+U approximations are almost of identical shape.

It is interesting to compare the spin and orbital moments obtained from the theoretically calculated XAS and XMCD spectra through sum rules [equation (3),(4)] with directly calculated LSDA+U values in order to avoid exra experimental problems. The number of the transition metal 3d electrons is calculated by integrating the occupied d partial density of states inside the corresponding atomic sphere which gives the values averaged for the nonequivalent sites $n_{\rm Co}$=7.742 and $n_{\rm Fe}$=6.542. Sum rules reproduce the spin magnetic moments within 31%, and 30% and the orbital moments within 35% and 34% for Co and Fe, respectively (Table 1). XMCD sum rules are derived within an ionic model using a number of approximations. For $L_{2,3}$, they are [48]: (1) neglecting the exchange splitting of the core levels; (2) replacing the interaction operator $\boldsymbol{\alpha} \cdot \mathbf{a}_\lambda$ in equation (1) by $\boldsymbol{\nabla} \cdot \mathbf{a}_\lambda$; (3) neglecting the asphericity of the core states; (4) neglecting the difference of $d_{3/2}$ and $d_{5/2}$ radial wave functions; (5) neglecting $p \to s$ transitions; (6) neglecting the energy dependence of the radial matrix elements. To effect the effect of the last point we applied the sum rules to the XMCD spectra neglecting the energy dependence of the radial matrix elements. As can be seen in Table 1 using the energy independent radial matrix elements, the disagreement in spin magnetic moments is reduced to 6% and 11% and in the orbital moment to 1% and 3% for Co and Fe, respectively. Moreover, the omission of the $p \to s$ transitions leads to a quite good agreement between the LSDA+U and sum rule results (within 4% and 10% for the spin moments at the Co and Fe sites, respectively, and less than 1% for the orbital moments for both sites). These results show that the energy dependence of the matrix elements and the presence of $p \to s$ transitions strongly affect the values of both the spin and the orbital magnetic moments derived from the sum rules.

4. Summary

We have studied the electronic structure and x-ray magnetic circular dichroism spectra of the Heusler alloy Co_2FeSi by means of an *ab initio* fully-relativistic spin-polarized Dirac linear muffin-tin orbital method.

The spin-polarized LSDA+U calculations without the SO coupling show that Co_2FeSi is a half-metallic ferromagnet. The calculated total DOS shows a gap of 1.0 eV for minority spin electrons. The gap in the minority bands is due to the Co–Fe interactions as the strongest bonding interactions. The spin-orbit coupling destroys the energy gap in the minority-spin states. Nevertheless, the spin polarization of electron states at the Fermi energy in the Heusler alloys Co_2FeSi is still high (about 95%).

The band structure calculations in the LSDA+U approximation reproduce quite well the shape of the XAS and XMCD spectra at the Co and Fe $L_{2,3}$ edges. The energy dependence of the matrix elements as well as the presence of $p \to s$ transitions strongly affect the values of both the spin and the orbital magnetic moments derived from the calculated XAS and XMCD spectra using the sum rules.

References

1. Prinz G.A., Science, 1998, **282**, 1660.
2. Wolf S.A., Awschalom D.D., Buhrman R.A., Daughton J.M., von Molnar S., Roukes M.L., Chtchelkanova A., Treger D.M., Science, 2001, **294**, 1488.
3. de Groot R.A., Mueller F.M., van Engen P.G., Buschow K.H.J., Phys. Rev. Lett., 1983, **50**, 2024.
4. Balke B., Wurmehl S., Fecher G., Felser C., Alves M., Bernardi F., Morais J., Applied Physics Letters, 2007, **90**, 172501.
5. Balke B., Fecher G.H., Kandpal H.C., Felser C., Kobayashi K., Ikenaga E., Kim J.-J., Ueda S., Phys. Rev. B, 2006, **74**, 104405.
6. Wurmehl S., Fecher G., Kandpal H., Ksenofontov V., Felser C., Lin H., Morais J., Phys. Rev. B, 2005, **72**, 184434.
7. Schneider H., Jakob G., Kallmayer M., Elmers H. J., Cinchetti M., Balke B., Wurmehl S., Felser C., Aeschlimann M., Adrian H., Phys. Rev. B, 2006, **74**, 174426.
8. Gloskovskii A., Barth J., Balke B., Fecher G., Felser C., Kronast F., Ovsyannikov R., Dürr H., Eberhard W., Schönhense G., J. Phys. D: Appl. Phys., 2007, **40**, 1570–1575.
9. Inomata K., Okamura S., Miyazaki A., Tezuka N., Wojcik M., Jedryka E., J. Phys. D: Appl. Phys., 2006, **39**, 816.
10. Kandpal H., Fecher G., Felser C., Schönhense G., Phys. Rev. B, 2006, **73**, No. 9, 094422.
11. Nakatani T.M., Rajanikanth A., Gercsi Z., Takahashi Y. K., Inomata K., Hono K., J. Appl. Phys., 2007, **102**, 033916.
12. Moruzzi V.L., Janak J.F., Williams A.R. Calculated Electronic Properties of Metals. Pergamon, New York, 1978.
13. von Barth U., Hedin L., J. Phys. C, 1972, **5**, 1629.
14. Vosko S.H., Wilk L., Nusair M., Can. J. Phys., 1980, **58**, 1200–1211.
15. Engel E., Vosko S.H., Phys. Rev. B, 1993, **47**, 13164.
16. Perdew J.P., Phys. Rev. B, 1986, **33**, 8822.
17. Perdew J.P., Yue W., Phys. Rev. B, 1986, **33**, R8800.
18. Sargolzaei M., Richter M., Koepernik K., Opahle I., Eschrig H., Chaplygin I., Phys. Rev. B, 2006, **74**, 224410.
19. Kleiner W.H. Phys. Rev., 1966, **142**, 318.
20. Richtmyer F.K., Barnes S.W., Ramberg E., Phys. Rev., 1934, **46**, 843.
21. Anisimov V.I., Zaanen J., Andersen O.K., Phys. Rev. B, 1991, **44**, 943.
22. Yaresko A.N., Antonov V.N., Fulde P., Phys. Rev. B, 2003, **67**, 155103.
23. van der Laan G., Thole B.T., Phys. Rev. B, 1988, **38**, 3158.
24. Thole B.T., Carra P., Sette F., van der Laan G., Phys. Rev. Lett., 1992, **68**, 1943.
25. Carra P., Thole B.T., Altarelli M., Wang X., Phys. Rev. Lett., 1993, **70**, 694.
26. van der Laan G., Thole B.T., Phys. Rev. B, 1996, **53**, 14458.
27. Antonov V., Harmon B., Yaresko A. Electronic structure and magneto-optical properties of solids. Kluwer Academic Publishers, Dordrecht, Boston, London, 2004.
28. Antonov V.N., Harmon B.N., Yaresko A.N., Phys. Rev. B, 2001, **63**, 205112.
29. Antonov V.N., Harmon B.N., Yaresko A.N., Phys. Rev. B, 2002, **66**, 165208.
30. Antonov V.N., Harmon B.N., Yaresko A.N., Phys. Rev. B, 2002, **66**, 165209.
31. Antonov V.N., Harmon B.N., Andryushchenko O., Bekenev L., Yaresko A.N., Low Temp. Phys., 2004, **30**, 411–426.
32. Niculesku V., Burch T., Raj K., Budnick J., J. Magn. Magn. Mater., 1977, **5**, 60–66.
33. Andersen O.K., Phys. Rev. B, 1975, **12**, 3060.
34. Nemoshkalenko V.V., Krasovskii A.E., Antonov V.N., Antonov V.N., Fleck U., Wonn H., Ziesche P., Phys. Status Solidi B, 1983, **120**, 283–296.
35. Perdew J.P., Wang Y., Phys. Rev. B, 1992, **45**, 13244–13249.
36. Blöchl P.E., Jepsen O., Andersen O.K., Phys. Rev. B, 1994, **49**, 16223.
37. Fuggle J.C., Inglesfield J.E. Unoccupied Electronic States. Topics in Applied Physics, vol. 69. Springer, New York, 1992.
38. Mavropoulos1 P., Galanakis I., Popescu V., Dederichs P.H., J. Phys.: Condens. Matter, 2004, **16**, S5759–S5762.
39. Mavropoulos P., Sato K., Zeller R., Dederichs P. H., Popescu V., Ebert H., Phys. Rev. B, 2004, **69**, 054424.
40. Schwitalla J., Ebert H., Phys. Rev. Lett., 1998, **80**, 4586.

41. Scott G.G., J. Phys. Soc. Jpn., 1962, **17**, 372.
42. Marshall W., Lovsey S.W. Theory of Thermal Neutron Scattering. Oxford University Press, Oxford, 1971.
43. Blume M., J. Appl. Phys., 1985, **57**, 3615.
44. Tjeng L.H., Chen C.T., Rudolf P., Meigs G., van der Laan G., Thole B.T., Phys. Rev. B, 1994, **48**, 13378.
45. Zaanen J., Sawatzky G.A., Fink J., Speier W., Fuggle J.C., Phys. Rev. B, 1985, **32**, 4905.
46. Böske T., Clemens W., Carbone C., Eberhardt W., Phys. Rev. B, 1994, **49**, 4003–4009.
47. Chen C.T., Idzerda Y.U., Lin H.-J., Smith N.V., Meigs G., Chaban E., Ho G.H., Pellegrin E., Sette F., Phys. Rev. Lett., 1995, **75**, 152.
48. Ebert H., Rep. Prog. Phys., 1996, **59**, 1665–1735.
49. Vignale G., Rasolt M., Phys. Rev. Lett., 1987, **59**, 2360.
50. Skudlarski P., Vigmale G., Phys. Rev. B, 1993, **48**, 8547.
51. Higuchi M., Haegawa A., J. Phys. Soc. Jpn., 1997, **66**, 149.
52. Brooks M.S.S., Physica B, 1985, 130, 6.
53. Eriksson O., Brooks M.S.S., Johansson B., Phys. Rev. B, 1990, **41**, 7311.
54. Severin L., Brooks M.S.S., Johansson B., Phys. Rev. Lett., 1993, **71**, 3214.
55. Mavromaras A., Sandratskii L., Kübler J., Solid State Commun., 1998, **106**, 115.
56. Beiden S.V., Temmerman W.M., Szotek Z., Gehring G.A., Phys. Rev. Lett., 1997, **79**, 3970.
57. Solovyev I.V., Liechtenstein A.I., Terakura K., Phys. Rev. Lett., 1998, **80**, 5758–5761.
58. Czyżyk M.T., Sawatzky G.A., Phys. Rev. B, 1994, **49**, 14211–14228.
59. Liechtenstein A.I., Anisimov V.I., Zaanen J., Phys. Rev. B, 1995, **52**, R5467–R5470.

Електронна структура та рентгенівський магнітний циркулярний дихроїзм хойслерівського сплаву Co_2FeSi

В.Н.Антонов[1], Д.А.Кукуста[1], А.П.Шпак[1], А.Н.Яресько[2]

[1] Інститут металофізики Національної Академії Наук України, бульвар Вернадського, 36, Київ, 03142
[2] Інститут Макса Планка фізики твердого тіла, Гейзенбергштрассе 1, 70569 Штуттгарт, Німеччина

Отримано 11 грудня 2007 р., в остаточному вигляді – 18 червня 2008 р.

Електронна структура та спектри рентгенівского магнітного циркулярного дихроїзму (РМЦД) хойслерівського сплаву Co_2FeSi були досліджені теоретично з перших принципів за допомогою повністю релятивістського Діраківського лінійного методу ЛМТО. Проаналізовані та обговорені щільності валентних електронів, орбітальні та магнітні спінові моменти, а також поляризація електронів на рівні Фермі.Вивчається походження спектрів РМЦД у Co_2FeSi. Результати обчислень порівнюються з еспериментальними даними.

Ключові слова: *сильно скорельовані системи, електронна структура, рентгенівский магнітний циркулярний дихроїзм*

PACS: *71.28.+d, 71.25.Pi, 75.30.Mb*